DOI: 10.1002/chem.200500295

Controlling Metal–Ligand–Metal Oxidation State Combinations by Ancillary Ligand (L) Variation in the Redox Systems $[L_2Ru(\mu\text{-boptz})RuL_2]^n$, boptz = 3,6-bis(2-oxidophenyl)-1,2,4,5-tetrazine, and L = acetylacetonate, 2,2′-bipyridine, or 2-phenylazopyridine

Srikanta Patra,[a] Biprajit Sarkar,[b] Somnath Maji,[a] Jan Fiedler,[c] Francisco A. Urbanos,[d] Reyes Jimenez-Aparicio,*[d] Wolfgang Kaim,*[b] and Goutam Kumar Lahiri*[a]

Abstract: The new compounds $[(acac)_2Ru(\mu\text{-boptz})Ru(acac)_2]$ (**1**), $[(bpy)_2Ru(\mu\text{-boptz})Ru(bpy)_2](ClO_4)_2$ (**2**-$(ClO_4)_2$), and $[(pap)_2Ru(\mu\text{-boptz})Ru(pap)_2](ClO_4)_2$ (**3**-$(ClO_4)_2$) were obtained from 3,6-bis(2-hydroxyphenyl)-1,2,4,5-tetrazine (H_2boptz), the crystal structure analysis of which is reported. Compound **1** contains two antiferromagnetically coupled ($J = -36.7\ cm^{-1}$) Ru^{III} centers. We have investigated the role of both the donor and acceptor functions containing the $boptz^{2-}$ bridging ligand in combination with the electronically different ancillary ligands (donating $acac^-$, moderately π-accepting bpy, and strongly π-accepting pap; acac = acetylacetonate, bpy = 2,2′-bipyridine pap = 2-phenylazopyridine) by using cyclic voltammetry, spectroelectrochemistry and electron paramagnetic resonance (EPR) spectroscopy for several in situ accessible redox states. We found that metal–ligand–metal oxidation state combinations remain invariant to ancillary ligand change in some instances; however, three isoelectronic paramagnetic cores Ru(μ-boptz)Ru showed remarkable differences. The excellent tolerance of the bpy coligand for both Ru^{III} and Ru^{II} is demonstrated by the adoption of the mixed-valent form in $[L_2Ru(\mu\text{-boptz})RuL_2]^{3+}$, L = bpy, whereas the corresponding system with pap stabilizes the Ru^{II} states to yield a phenoxyl radical ligand and the compound with L = $acac^-$ contains two Ru^{III} centers connected by a tetrazine radical-anion bridge.

Keywords: bridging ligands · EPR spectroscopy · magnetic properties · N,O ligands · ruthenium

[a] S. Patra, S. Maji, Prof. Dr. G. K. Lahiri
Department of Chemistry, Indian Institute of Technology Bombay
Powai, Mumbai 400076 (India)
Fax: (+91) 022-2572-3480
E-mail: lahiri@chem.iitb.ac.in

[b] Dr. B. Sarkar, Prof. Dr. W. Kaim
Institut für Anorganische Chemie, Universität Stuttgart
Pfaffenwaldring 55, 70550 Stuttgart (Germany)
Fax: (+49) 711-685-4165
E-mail: kaim@iac.uni-stuttgart.de

[c] Dr. J. Fiedler
J. Heyrovský Institute of Physical Chemistry
Academy of Sciences of the Czech Republic, Dolejškova 3
18223 Prague (Czech Republic)

[d] Dr. F. A. Urbanos, Dr. R. Jimenez-Aparicio
Departamento de Química Inorgánica
Facultad de Ciencias Químicas, Universidad Complutense
Ciudad Universitaria, 28040 Madrid (Spain)
Fax: (+34) 91-394-4352
E-mail: qcmm@quim.ucm.es

Supporting information for this article is available on the WWW under http://www.chemeurj.org/ or from the authors.

Introduction

Intramolecular electron transfer is of importance for redox reactivity[1,2] and for some concepts of molecular electronics.[2] Molecule-bridged dinuclear complexes, especially mixed-valent compounds,[1,3] have played an important role in understanding intramolecular electron transfer and its control through external factors such as the ancillary (terminal) ligands L in systems of the general composition $[L_nM^m(\mu\text{-BL})M^{m+1}L_n]^k$ (BL: bridging ligand). However, beyond the tuning of the extent of electronic coupling between mixed-valent metal centers[3] through electron- or hole-transfer mechanisms,[4,5] one may also envisage full participation of the bridge in electron exchange by forming ligand-reduced species $[L_nM^{m+1}(\mu\text{-BL}^{\bullet-})M^{m+1}L_n]^k$ or ligand-oxidized forms $[L_nM^m(\mu\text{-BL}^{\bullet+})M^mL_n]^k$.

Bridging ligands that are capable of both reversible and facile oxidation and reduction are uncommon. Here we present the analysis of diruthenium systems $[L_2Ru(\mu\text{-boptz})$-

$RuL_2]^n$, $boptz^{2-}$ = 3,6-bis(2-oxidophenyl)-1,2,4,5-tetrazine and L = $acac^-$ (acetylacetonate, donor), bpy (2,2′-bipyridine, weak π-acceptor), or pap (2-phenylazopyridine, strong π-acceptor).[6]

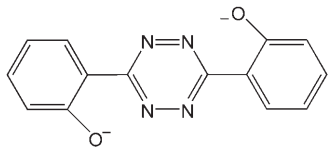

$boptz^{2-}$

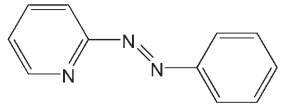

pap

The new symmetrically bis(bidentate) bridging ligand $boptz^{2-}$ contains two phenolate donors and a central tetrazine π-acceptor function, each bonding to both metals in a dinuclear configuration. Phenolates are capable of coordination-supported oxidation to biochemically relevant phenoxyl radicals that are known to be stabilized by metal bonding.[7] On the other hand, 3,6-disubstituted-1,2,4,5-tetrazine moieties have become popular as efficient electronic spacers in dinuclear and polynuclear systems.[8] This is primarily due to the fact that the tetrazine-based low-lying π* orbital conveys strong π-accepting characteristics, leading to excellent electronic communication between the metal termini. This discovery has spurred the design of a number of dinuclear ruthenium complexes with a wide variation of molecular frameworks.[9] 3,6-Bis(2-pyridyl)-1,2,4,5-tetrazine (bptz) in particular has been used extensively in synthesizing diruthenium complexes $[L_nRu(\mu\text{-bptz})RuL_n]^k$ in combination with ancillary ligands L of varying electronic nature such as NH_3,[9a,b] bpy,[9c] $acac^-$,[9d] [9]aneS$_3$ (1,4,7-trithiacyclononane),[9e] or arenes.[9t] Considerable variation has been observed for the comproportionation constants (K_c) of the $Ru^{III}Ru^{II}$ mixed-valent intermediates in those complexes, based on the electronic properties of the ancillary ligands: K_c: 1×10^{15} (L = NH_3); 3×10^{8} (L = bpy); 1×10^{13} (L = $acac^-$); 1.4×10^{8} (L = [9]aneS$_3$). Similarly, the modified framework of the tetrazine-based spacer 3,6-bis(3,5-dimethylpyrazolyl)-1,2,4,5-tetrazine (bpytz) also exhibits a substantial difference in K_c, depending on the ancillary ligands ($K_c = 10^{7.6}$ or $10^{13.9}$ for L = bpy[9n] or $acac^-$,[9s] respectively). In addition, other 3,6-disubstituted tetrazine-based bridging ligands such as 3,6-bis(2-thienyl)-1,2,4,5-tetrazine (bttz),[9m] 3,6-bis(4-methyl-2-pyridyl)-1,2,4,5-tetrazine (bmptz),[9m] and 3,6-bis(carbomethoxy)-1,2,4,5-tetrazine (bctz)[9c] have also been utilized in developing diruthenium complexes incorporating π-acidic bpy co-ligands.

Although a fairly large number of diruthenium complexes have been synthesized by using tetrazine-based neutral spacers, analogous complexes of corresponding anionic derivatives are not known. The present work deals with the doubly deprotonated form of 3,6-bis(2-hydroxyphenyl)-1,2,4,5-tetrazine (H_2boptz). The observed substantial effects of ancillary ligands on the mixed-valent properties of bptz- and bpytz-bridged $Ru^{III}Ru^{II}$ species has prompted us to examine the effect of three electronically different ancillary functions, namely, $acac^-$ (σ-donating), bpy (moderately π-acidic), and pap (strongly π-acidic), on the extent of intermolecular electron-exchange processes in $boptz^{2-}$-bridged diruthenium species.

Here we report the syntheses of 3,6-bis(2-hydroxyphenyl)-1,4-dihydro-1,2,4,5-tetrazine (H_4boptz), its oxidized form 3,6-bis(2-hydroxyphenyl)-1,2,4,5-tetrazine (H_2boptz), and of the complexes $[(acac)_2Ru(\mu\text{-boptz})Ru(acac)_2]$ (**1**), $[(bpy)_2Ru(\mu\text{-boptz})Ru(bpy)_2](ClO_4)_2$ (**2**-$(ClO_4)_2$) and $[(pap)_2Ru(\mu\text{-boptz})Ru(pap)_2](ClO_4)_2$ (**3**-$(ClO_4)_2$). We describe the crystal structure of the free ligand (H_2boptz), and have investigated the role of $boptz^{2-}$ in combination with the electronically different three ancillary ligands for the tuning of oxidation state configurations by using spectroelectrochemistry and EPR spectroscopy.

Results and Discussion

The free ligands 3,6-bis(2-hydroxyphenyl)-1,4-dihydro-1,2,4,5-tetrazine (H_4boptz) and its oxidized form 3,6-bis(2-hydroxyphenyl)-1,2,4,5-tetrazine (H_2boptz) were synthesized through the reaction of 2-hydroxybenzonitrile with hydrazine hydrate in refluxing ethanol and through the oxidation of H_4boptz by using NO gas, respectively.

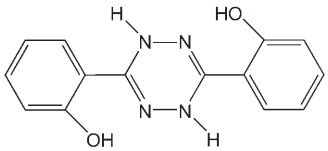

H_4boptz

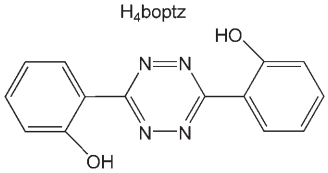

H_2boptz

The formation of H_2boptz was confirmed by single-crystal X-ray diffraction structure analysis (Figure 1). Selected crystallographic and bond parameters are listed in Tables 1 and 2, respectively. The structural parameters match well with reported values for related compounds.[9u] There is intramolecular hydrogen bonding between the hydroxy function O1−H1 and the neighboring tetrazine nitrogen atom N1 (*d*-(O···N), 2.631(2) Å and O−H···N, 145(3)°, Figure S1 and

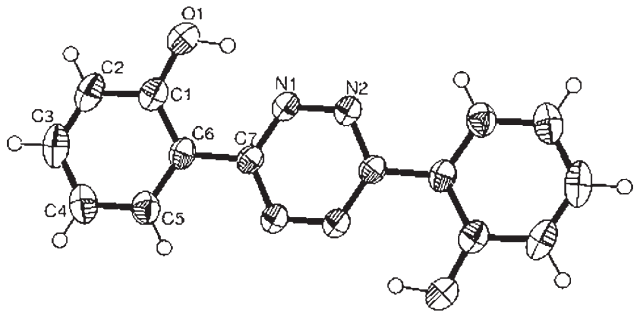

Figure 1. Crystal structure of H_2boptz. Ellipsoids are drawn at the 50% probability level.

Table 1. Crystallographic data for H_2boptz.

formula	$C_{14}H_{10}N_4O_2$
M_r	266.26
crystal size [mm]	0.40×0.35×0.30
crystal system	monoclinic
space group	$P21/c$
Z	2
a[Å]	4.5260 (8)
b[Å]	10.5570 (7)
c[Å]	12.4990 (11)
α[°]	90
β[°]	96.279 (10)
γ[°]	90
V[Å^3]	593.63 (12)
ρ_{calcd} [g cm^{-3}]	1.490
T[K]	293 (2)
μ[mm^{-1}]	0.105
F(000)	276
hkl range	h: 0–5; k: 0–12; l: −14–14
θ range [°]	2.53–24.92
measured reflections	1189/1050
unique reflections	1050 [R(int) = 0.0114]
observed reflections [$I>2\sigma(I)$]	1050
parameters	95
R_1	0.0419
wR_2	0.1115
R(all)	0.0618
residual electron density [e Å^{-3}]	0.290/−0.20

Table 2. Selected bond lengths [Å] and angles [°] for H_2boptz.

Bond lengths		Bond angles	
O1−C1	1.340(3)	N2-N1-C7	119.68(14)
N1−N2	1.313(2)	N1-N2-C7#1	117.46(15)
N1−C7	1.342(2)	O1-C1-C2	116.65(18)
N2−C7#1	1.340(2)	O1-C1-C6	124.20(17)
		N2#1-C7-N1	122.86(15)
		N2#1-C7-C6	118.39(16)
		N1-C7-C6	118.75(15)

Table S1 in the Supporting Information). The paramagnetic complex [{(acac)$_2$Ru^{III}}$_2$(μ-boptz^{2-})] (**1**) and the diamagnetic complexes [{(bpy)$_2$Ru^{II}}$_2$(μ-boptz^{2-})](ClO$_4$)$_2$ (**2**-(ClO$_4$)$_2$) and [{(pap)$_2$Ru^{II}}$_2$(μ-boptz^{2-})](ClO$_4$)$_2$ (**3**-(ClO$_4$)$_2$) were prepared from reactions of [Ru(acac)$_2$(CH$_3$CN)$_2$], [Ru(bpy)$_2$-(EtOH)$_2$]$^{2+}$, or [Ru(pap)$_2$(EtOH)$_2$]$^{2+}$, respectively, with H_2boptz in 2:1 molar ratio in the presence of excess NaOOCCH$_3$ (Scheme 1). Dianionic boptz^{2-} symmetrically

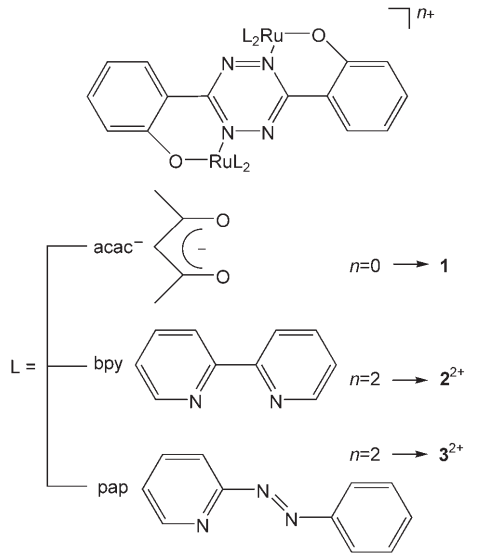

Scheme 1.

bridges two units of the metal complex fragments [Ru^{III}-(acac)$_2$]$^+$, [Ru^{II}(bpy)$_2$]$^{2+}$, or [Ru^{II}(pap)$_2$]$^{2+}$ in complexes **1**, **2**$^{2+}$, or **3**$^{2+}$, respectively, through the phenolate O$^-$ and tetrazine N-donor centers. While the +2 oxidation state of ruthenium in the precursors is retained in complexes **2**$^{2+}$ and **3**$^{2+}$, the Ru^{II} state of the precursor is oxidized to the +3 state in complex **1**, presumably by air. The presence of electron-rich acac$^-$ ancillary ligands in complex **1** as opposed to the moderately π-acidic bpy in complex **2**$^{2+}$ or strongly π-acidic pap in complex **3**$^{2+}$ facilitates the stabilization of the Ru^{III} state in complex **1** and this is also reflected in the redox potential data (see later).

We identified complexes **1**, **2**-(ClO$_4$)$_2$, and **3**-(ClO$_4$)$_2$ by microanalysis, molar conductance, and electrospray (ESI) mass spectrometry (see Experimental Section). They were further investigated in various oxidation states (see below) by using cyclic voltammetry, spectroelectrochemistry, and EPR spectroscopy. We studied the magnetism of paramagnetic **1** by using superconducting quantum interface device (SQUID) susceptometry.

The diamagnetic complexes **2**$^{2+}$and **3**$^{2+}$ displayed complicated ^{1}H NMR spectra due to overlap of 40 and 44 signals, respectively, with rather similar chemical shifts in the aromatic region. The ^{1}H NMR spectrum of complex **2**$^{2+}$ indicates the presence of a mixture of two isomers (*meso* and *rac*),[9h,10] in a ratio of approximately 2:1 that we failed to separate even by preparatory TLC. Whereas redox potentials and absorption spectra are only marginally different for such isomers,[10] the EPR characteristics of paramagnetic forms are more sensitive in that respect (see EPR Section below).

We carried out variable-temperature (2–300 K) magnetic studies of a powder sample of complex **1**. The magnetic susceptibility curve versus temperature shows a broad maximum at 64 K (Figure 2), implying bridging-ligand-mediated antiferromagnetic interaction between the Ru^{III} centers. In

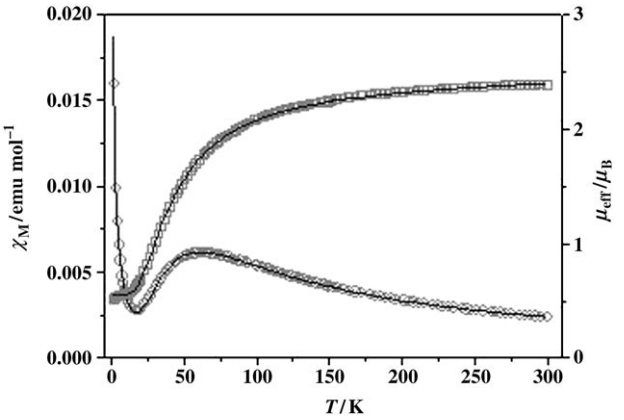

Figure 2. Temperature-dependence of the molar susceptibility χ_M (○) and μ_{eff} (□) for **1**. Solid lines are the products of a least-squares fit to the model mentioned in the text.

addition, we observe a tail in the low-temperature end that suggests the presence of a paramagnetic impurity.

The gradual decrease of the magnetic moment of complex **1** from 2.38 μ_B at 300 K to 0.55 μ_B at 10 K confirms the existence of bridging-ligand-mediated antiferromagnetic interaction between the Ru^{III} centers. The slight decrease of μ from 0.55 to 0.51 μ_B in the temperature range of 10–2 K suggests the presence of a paramagnetic species without antiferromagnetic coupling (Figure 2). The magnetic behavior of complex **1** can be explained with a model that takes into account the effects of an exchange spin Hamiltonian $\mathscr{H} = -2JS_1 \cdot S_2$ where $S_1 = S_2 = {}^1/_2$, with intramolecular antiferromagnetic coupling between the Ru^{III} centers.[11] In addition, temperature-independent paramagnetism (TIP) has been included as is usual in ruthenium complexes [Eq. (1)]. Moreover, a dimeric species with two uncoupled Ru^{III} centers ($S=1$, $g=2$) has been considered as a possible source for paramagnetic impurities.

$$\chi = \frac{Ng^2\beta^2}{kT}\frac{2\exp(2J/kT)}{1+3\exp(2J/kT)} + \mathrm{TIP} \qquad (1)$$

The fit of the experimental data with Equation (2) gives excellent agreement of the calculated and experimental magnetic moment and susceptibility curves (Figure 2). The parameters obtained in the best fits are: $g=2.0$, $J=-36.7\ cm^{-1}$, $TIP=1.1\times10^{-4}\ emu\,mol^{-1}$, $P=3.7\,\%$, and $\sigma^2=3.4\times10^{-5}$ ($\sigma^2=\Sigma(\mu_{eff\,calcd}-\mu_{eff\,exptl})^2/\Sigma\mu^2_{eff\,exptl}$). The calculated g and TIP values are typical for ruthenium complexes.[12–14]

$$\chi' = (1-P)\chi + P\frac{2Ng^2\beta^2}{3kT} \qquad (2)$$

The J value of $-36.7\ cm^{-1}$ for complex **1** is similar to that reported for $[L(acac)Ru(\mu\text{-}O)Ru(acac)L](PF_6)_2$ (L = 1,7-trimethyl-1,4,7-triazacyclononane) ($J=-53\ cm^{-1}$) that has a Ru-O-Ru angle of 180°,[12] but much higher than that observed in $[(acac)_2Ru(\mu\text{-}(NC_5H_4)_2N\text{-}C_6H_4\text{-}N\text{-}(NC_5H_4)_2)Ru(acac)_2](ClO_4)_2$ ($J=-0.45\ cm^{-1}$) or $[(acac)_2Ru(\mu\text{-}OC_2H_5)_2Ru(acac)_2]$ ($J=-0.63\ cm^{-1}$).[13] In contrast, the J for complex **1** is much lower than that observed in several (μ-alkoxo)bis(μ-carboxylato)diruthenium(III) complexes ($J=-310$ to $-728\ cm^{-1}$).[14]

Electrochemistry and EPR spectroscopy: In CH_3CN, the paramagnetic $Ru^{III}Ru^{III}$ complex **1** exhibits two successive one-electron oxidation waves (Figure 3a, Table 3) and a

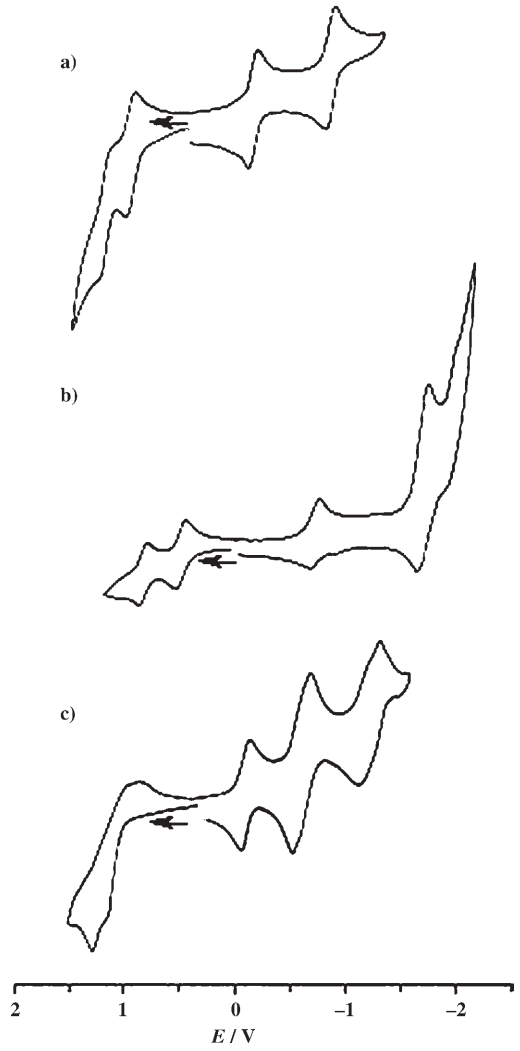

Figure 3. Cyclic voltammograms of: a) **1** in CH_2Cl_2, b) **2**-$(ClO_4)_2$, and c) **3**-$(ClO_4)_2$ in CH_3CN at 298 K.

weak rhombic EPR signal at 4 K. Both the g anisotropy $g_1-g_3=0.636$ and the average $g_{av}=2.240$ from EPR spectroscopy are indicative of Ru^{III}-based spin (Table 4).[15] The half-field EPR signal expected for a triplet state was not observed under those conditions. This and the low intensity of the EPR response already suggest that the Ru^{III} centers in complex **1** are rather strongly coupled with antiparallel alignment of spins from the low-spin d^5 configurations. In

Table 3. Redox potentials of complexes[a].

$n/n-1$[b]	Couple	$E_{1/2}$ (ΔE_{pp})[c]	Couple	$E_{1/2}$ (ΔE_{pp})[c]	Couple	$E_{1/2}$ (ΔE_{pp})[c]
4/3			$\mathbf{2}^{4+}/\mathbf{2}^{3+}$	0.84 (70)	$\mathbf{3}^{4+}/\mathbf{3}^{3+}$	1.28[e]
3/2			$\mathbf{2}^{3+}/\mathbf{2}^{2+}$	0.48 (80)	$\mathbf{3}^{3+}/\mathbf{3}^{2+}$	1.14[e]
2/1	$\mathbf{1}^{2+}/\mathbf{1}^{+}$	1.19 (90)	$\mathbf{2}^{2+}/\mathbf{2}^{+}$	−0.75 (60)	$\mathbf{3}^{2+}/\mathbf{3}^{+}$	−0.10(70)
1/0	$\mathbf{1}^{+}/\mathbf{1}$	0.96 (90)	$\mathbf{2}^{+}/\mathbf{2}$	−1.76 (100)[d]	$\mathbf{3}^{+}/\mathbf{3}$	−0.56 (60)
0/−	$\mathbf{1}/\mathbf{1}^{-}$	−0.18 (80)			$\mathbf{3}/\mathbf{3}^{-}$	−0.67(60)
−/2−	$\mathbf{1}^{-}/\mathbf{1}^{2-}$	−0.89 (90)			$\mathbf{3}^{-}/\mathbf{3}^{2-}$	−1.17(60)
2−/3−					$\mathbf{3}^{2-}/\mathbf{3}^{3-}$	−1.30(60)

[a] From cyclic voltammetry in CH_2Cl_2 for **1** and in CH_3CN/0.1 M Et_4NClO_4 for **2** and **3**, at 50 mV s^{-1}. [b] Change in charge of the $[Ru(\mu\text{-boptz})Ru]^{(n/n-1)+}$ core. [c] In V versus SCE; peak potential differences ΔE_{pp} [mV] (in parentheses). [d] Further bpy-based reductions at −1.76 (100) and −2.02 V (80 mV). [e] Anodic peak potential (E_{pa}), process not fully reversible.

Table 4. EPR data of paramagnetic states.[a]

	g_1	g_2	g_3	g_{av}[b]	$\Delta g = g_1 - g_3$	K_c[c]
1[d]	2.543	2.224	1.907	2.240	0.636	7.9×10^3
$\mathbf{1}^{-}$[d]	2.220	2.220	1.743	2.073	0.477	1.1×10^{12}
$\mathbf{2}^{3+}$[d,e]	2.499	2.160	1.828	2.180	0.671	1.3×10^6
	2.328	2.160	1.878	2.130	0.450	
$\mathbf{2}^{+}$[g]	[f]	[f]	[f]	2.0034		
$\mathbf{3}^{3+}$[d,g]	2.022	1.999	1.999	2.0007[h]		
$\mathbf{3}^{+}$[g]	[f]	[f]	[f]	1.9946		

[a] From EPR spectroelectrochemical data in CH_3CN/0.1 M Bu_4NPF_6, except for **1**, g tensor components determined at 4 K. [b] $g_{av}=(1/3(g_1^2+g_2^2+g_3^2))^{1/2}$. [c] Comproportionation constant from $RT\ln K_c = nF(\Delta E)$; for ΔE see Table 3. [d] EPR measurements at 4 K. [e] Two isomers (*meso* and *rac*). [f] No g anisotropy measured. [g] EPR measurements at 298 K, ^{14}N hyperfine coupling of 0.5 mT. [h] $g_{iso}=2.0046$ at 298 K.

fact, SQUID susceptibility measurements reveal antiferromagnetic coupling.

Although an odd-electron system, the one-electron oxidized intermediate $\mathbf{1}^{+}$ did not show an EPR signal, even at 4 K. The rapid EPR relaxation suggests metal-centered spin(s) and close-lying excited states as may be anticipated for a $Ru^{IV}Ru^{III}$ (d^4/d^5) mixed-valent situation with possibly close-lying singlet and triplet states of the d^4 center. This EPR silence is in contrast to EPR observations made for other bridged bis(bis(acetylacetonato)ruthenium) complexes, which allow for a $Ru^{IV}(L^{2-})Ru^{III} \leftrightarrow Ru^{III}(L)Ru^{II}$ resonance.[16] The 230 mV separation between the oxidation couples for complex **1** leads to a comproportionation constant K_c of 7.9×10^3 (calculated by using the equation $RT\ln K_c = nF(\Delta E)$)[17] for the monocationic intermediate. This low value and the absence of an EPR signal for Ru^{IV}-(boptz^{2-})Ru^{III} suggest a Class II mixed-valent state.[18]

Complex **1** exhibits two one-electron reduction processes at −0.18 and −0.89 V versus SCE (Figure 3a, Table 3). The K_c value of 1.1×10^{12} for the $\mathbf{1}^{-}$ complex is much higher than that for the $\mathbf{1}^{+}$ complex, suggesting either tetrazine-centered reduction[8,9] or the formation of a strongly coupled $Ru^{III}Ru^{II}$ mixed-valent state.[4,18] The one-electron reduced species $\mathbf{1}^{-}$ displays an axial EPR signal with an average g_{av} factor of 2.073 and a g anisotropy $g_1-g_3=0.48$ (Figure 4a, Table 4), indicative of metal-centered spin. However, complex $\mathbf{1}^{-}$ does not show the NIR transition expected for a Ru^{III}-(boptz^{2-})Ru^{II} intermediate (see later). Thus, the reduced $\mathbf{1}^{-}$ complex can be best described by a three-spin situation,[19] Ru^{III}(boptz$^{\bullet3-}$)Ru^{III}, in which the ($S=1/2$) ground state involves dominant antiferromagnetic coupling between one of the Ru^{III} centers and boptz$^{\bullet3-}$,[19] leaving one metal-centered spin active for EPR.

With bpy as ancillary ligands the corresponding $Ru^{II}Ru^{II}$ compound $\mathbf{2}^{2+}$ exhibits two successive one-electron oxidation processes at 0.48 and 0.84 V versus SCE with $K_c=1.3\times10^6$ (Figure 3b, Table 3). The first-step oxidized species $\mathbf{2}^{3+}$ displays two sets of rhombic EPR spectra at 4 K (Figure 4b, Table 4). The corresponding g anisotropies g_1-g_3 are 0.67 and 0.45, respectively; the resulting g_{av} values are 2.180 and 2.130, respectively.

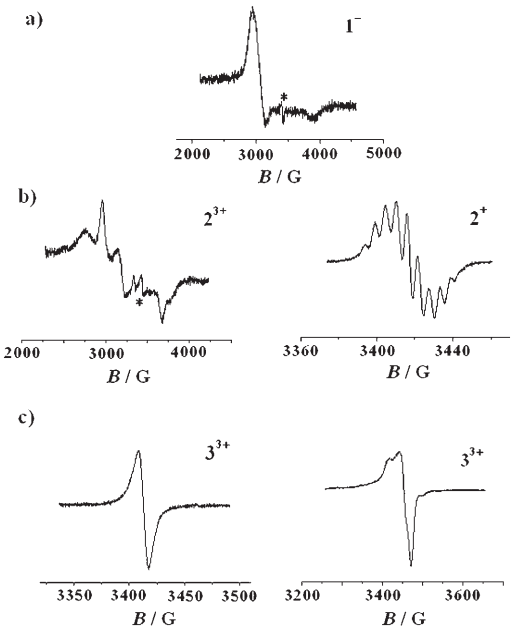

Figure 4. EPR spectra of: a) $\mathbf{1}^{-}$ in CH_2Cl_2 at 4 K, b) $\mathbf{2}^{3+}$ at 4 K (left) and $\mathbf{2}^{+}$ at 298 K (right), and c) $\mathbf{3}^{3+}$ at 298 K (left) and $\mathbf{3}^{3+}$ at 4 K (right) in CH_3CN (* denotes artifact signals due to the EPR cavity).

These observations reveal: 1) the presence of two isomeric forms (*meso* and *rac*), in the oxidized $\mathbf{2}^{3+}$ state with distinct electronic structures; 2) a metal-based oxidation corresponding to a Ru^{III}(boptz^{2-})Ru^{II} (or, better, $Ru^{2.5}$(boptz^{2-})$Ru^{2.5}$) formulation for the intermediate $\mathbf{2}^{3+}$; and 3) the Class III category for that intermediate. The Ru^{III}/Ru^{II} couples for complexes with the corresponding neutral tetrazine-based spacers bptz, bpytz, bmptz, and bttz appeared at 1.52, 2.2;[9c] 1.25, 1.70;[9n] 1.34, 1.87,[9m] and 0.68, 1.68 V,[9m] respectively. The dianionic boptz^{2-} ligand substantially destabilizes the Ru^{II} state in the $\mathbf{2}^{2+}$ complex. It should be noted that the combination of bpy ancillary ligands and neutral tetrazine-

based spacers also produced delocalized $Ru^{III}Ru^{II}$ states.[9c,n,m] Unlike these compounds with neutral tetrazine-centered spacers and mostly higher K_c values, however, the mixed-valent $\mathbf{2}^{3+}$ does not show a well-defined intervalence charge-transfer (IVCT) band in the NIR region, but only significantly enhanced absorption around and beyond 2000 nm (see later, Figure 6).

The tetrazine-based one-electron reduction of complex $\mathbf{2}^{2+}$ occurs at −0.75 V versus SCE in CH_3CN (Figure 3b). For the analogous bptz, bpytz, bmptz, and bttz complexes this process is observed at −0.03,[9c] −0.13,[9n] −0.21,[9m] and −1.02 V,[9m] respectively. Thus, the introduction of dianionic $boptz^{2-}$ ligand in complex $\mathbf{2}^{2+}$ in place of neutral tetrazines results in an appreciably destabilized LUMO.

The one-electron-reduced species $\mathbf{2}^{+}$ exhibits a typically resolved radical-type EPR spectrum[20] in CH_3CN at 298 K due to hyperfine splitting of approximately 0.5 mT from four ^{14}N atoms of the tetrazine ring of $boptz^{\bullet 3-}$. The spectrum is centered at $g=2.0034$ (Figure 4b, Table 4); both ruthenium atoms remain in the divalent state in complex $\mathbf{2}^{+}$.

In addition to a second reduction of the bridging ligand, complex $\mathbf{2}^{2+}$ also displays the expected multiple bpy-based reductions in the range between −1.76 and −2.02 V (Figure 3b, Table 3).[21]

The analogous complex $\mathbf{3}^{2+}$ with the stronger π-accepting pap[6] terminal ligands exhibits two closely spaced oxidation waves at 1.14 and 1.28 V versus SCE (Figure 3c, Table 3). Although even the first oxidation is not fully reversible on the timescale of cyclic voltammetry at room temperature, the one-electron-oxidized product could be obtained by intra muros electrolysis, displaying a sharp EPR signal at $g_{iso}=2.0046$ (298 K) indicative of free radicals (Figure 4c, Table 4), lying in a typical g_{iso} range for phenoxyl radicals;[7,22] the small but detectable axial g component splitting observed at 4 K (Figure 4c) is larger than that reported for uncoordinated phenoxyl (tyrosyl) radicals.[22] This observation suggests the formation of a metal-coordinated phenoxyl radical species $Ru^{II}(boptz^{\bullet -})Ru^{II}$ ($\mathbf{3}^{3+}$) instead of the otherwise conceivable mixed-valent alternative $Ru^{II}(boptz^{2-})Ru^{III}$ (which was observed for $\mathbf{2}^{3+}$). The formation of a phenoxyl radical complex is not only supported by the g factor from EPR spectroscopy and by the closeness of two less-reversible oxidation processes for two sterically unprotected, spatially separated, and only weakly coupled phenolate/phenoxyl redox pairs, further evidence comes from the appearance of a characteristic absorption band at 488 nm (see the Spectroelectrochemistry Section below).[7]

Both the tetrazine[8,9] part of $boptz^{2-}$ and the azo function of pap[6] are susceptible to undergo facile and often reversible reduction processes. The complex ion $\mathbf{3}^{2+}$ thus shows multiple reduction waves within the potential limit of −2.0 V versus SCE (Figure 3c, Table 3). The first-step reduced species $\mathbf{3}^{+}$ displays the familiar (see Figure 4b) nine-line EPR spectrum with a g_{iso} value centered at 1.9946 at 298 K. This, along with the corresponding coupling constant of about 0.5 mT from the EPR spectra simulation confirms[20] that the LUMO is primarily dominated by the tetrazine ring of the bridge in complex $\mathbf{3}^{+}$, formulated according to $Ru^{II}(boptz^{\bullet 3-})Ru^{II}$. The subsequent two sets of closely spaced reduction waves at −0.56, −0.67 and −1.17, −1.30 V versus SCE (Figure 3c and Table 3) can be tentatively assigned as successive reduction processes involving the 2-phenylazopyridine ancillary ligands.[6]

Spectroelectrochemistry: We investigated the absorption spectra of reversibly accessible states in the UV, visible, and NIR regions with an optically transparent thin-layer electrolysis (OTTLE) cell[23] in order to confirm the above assignments based on EPR data, to assign oxidation state combinations for the EPR-silent species, and to obtain information on the electronic structures in general. Due to the combined (phenolate) donor and (tetrazine) acceptor character of the bridging ligands, and because of the ancillary ligands containing conjugated-π systems, a large number of charge-transfer transitions can be expected at rather low energies. Assignments are therefore tentative and will have to be confirmed by quantum chemical calculations at a later stage. Unless stated otherwise, the results involve fully reversible transitions as confirmed by 100% spectra regeneration and the occurrence of isosbestic points. The spectra are shown in Figures 5–7, and spectral data are summarized in Table 5.

Table 5. UV-visible-NIR data of complexes from spectroelectrochemical data[a].

	λ_{max} [nm] (ε [$M^{-1}cm^{-1}$])
$\mathbf{1}^{+}$	830(sh), 690(11600), 397(12200), 304(22600), 265(21800), 242(21100)
1	815(6700), 620(sh), 560(9770), 455(10260), 390(sh), 355(14700), 297(19800), 270(19600), 240(18550)
$\mathbf{1}^{-}$	626(10270), 540(10250), 365(17300), 290(19300), 268(19900), 242(18600)
$\mathbf{1}^{2-}$	895(13300), 625(9900), 460(sh), 367(16000), 292(17600), 266(17800), 240(17500)
$\mathbf{2}^{4+}$	1350(sh), 1040(sh), 900(broad sh) (4000), 560(14300), 447(sh), 375(12000), 304(20400), 265(19000), 240(18500)
$\mathbf{2}^{3+}$	2000(broad sh), 1300(sh), 900(sh), 652(12950), 386(12750), 302(20200), 267(19200), 243(18300)
$\mathbf{2}^{2+}$	980(broad sh), 685(13300), 488(12750), 360(14900), 302(20200), 269(19700), 243(18900)
$\mathbf{2}^{+}$	675(sh), 545(11300), 483(11600), 374(13900), 300(19750), 267(19100), 242(18400)
$\mathbf{3}^{3+}$	1105(13900), 655(15300), 488(19500), 368(28500), 275(25000), 235(25600)
$\mathbf{3}^{2+}$	890(sh), 705(sh), 617(10700), 505(15200), 349(27900), 305(29300), 240(29200)
$\mathbf{3}^{+}$	1600(800), 725(sh), 572(8700), 485(9300), 345(25600), 300(25600), 240(29100)
3	1600(800), 575(8100), 352(26800), 303(23800), 240(29100)

[a] Solvent: CH_2Cl_2 for **1** and CH_3CN for **2**-$(ClO_4)_2$ and **3**-$(ClO_4)_2$.

Compound **1** exhibits intense bands at long wavelengths due to ligand-to-metal charge-transfer (LMCT) transitions expected for $Ru^{III}(boptz^{2-})Ru^{III}$. On oxidation to $Ru^{IV}(boptz^{2-})Ru^{III}$ the absorption in the 600–900 nm region intensifies (Figure 5a) and there appears to be increased absorption in the NIR region; however, no proper IVCT band

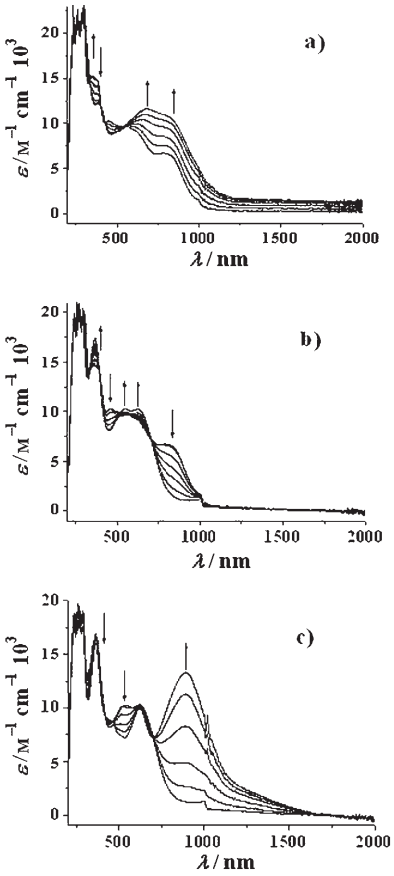

Figure 5. UV-visible-NIR spectroelectrochemistry for the conversions: a) $\mathbf{1}\rightarrow\mathbf{1}^{+}$, b) $\mathbf{1}\rightarrow\mathbf{1}^{-}$, and c) $\mathbf{1}^{-}\rightarrow\mathbf{1}^{2-}$ in CH_2Cl_2/0.1 M Bu_4NPF_6.

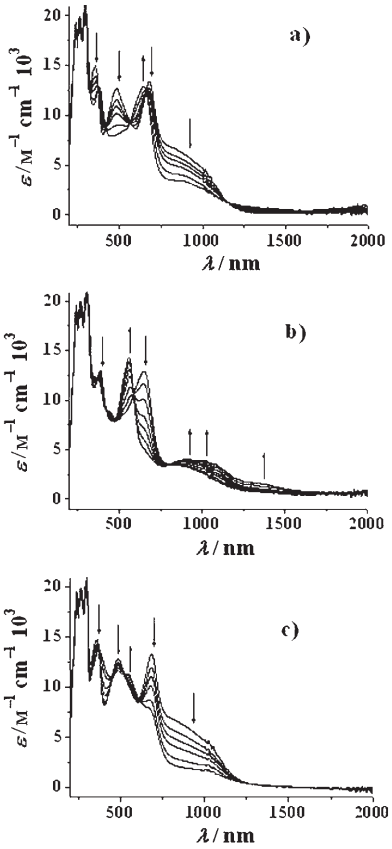

Figure 6. UV-visible-NIR spectroelectrochemistry for the conversions: a) $\mathbf{2}^{2+}\rightarrow\mathbf{2}^{3+}$, b) $\mathbf{2}^{3+}\rightarrow\mathbf{2}^{4+}$, and c) $\mathbf{2}^{2+}\rightarrow\mathbf{2}^{+}$ in CH_3CN/0.1 M Bu_4NPF_6.

was observed in agreement[24] with a weakly coupled mixed-valent situation (Figure 5a). The first reduction to Ru^{III}-(boptz$^{\bullet 3-}$)Ru^{III} results in the disappearance of the long-wavelength band that is typical for tetrazine radical compounds.[9q] The second reduced species $\mathbf{1}^{2-}$ exhibits a strong absorption band in the low-energy region (895 nm, $\varepsilon =$ 13300 $M^{-1}cm^{-1}$), compatible with an LMCT transition as expected for Ru^{III}(boptz^{4-})Ru^{III}. However, the alternate valence description of Ru^{II}(boptz^{2-})Ru^{II} with a low-lying MLCT transition[9] may not be ruled out.

The complex ion $\mathbf{2}^{2+}$ shows MLCT transitions around 700 and 480 nm to the π* orbitals of tetrazine and bpy as expected for a Ru^{II}(boptz^{2-})Ru^{II} situation (Figure 6).[9] The bathochromic shift for d(Ru)→π*(bpy) results from the coordination of an anionic phenolate that destabilizes the metal d orbitals. The mixed-valent $\mathbf{2}^{3+}$ complex ion containing Ru^{III}(boptz^{2-})Ru^{II} does not have a well-defined IVCT band in the NIR region; however, the absorption band significantly increases around and beyond 2000 nm (Figure 6a). Bis(chelate) and especially tetrazine-bridged mixed-valent intermediates have rather weak IVCT band intensities despite very large K_c values,[4,9b] the somewhat lower K_c value for the present case signified already attenuated metal–metal interactions that would be compatible with a further decreased IVCT absorption. The second oxidation to give a Ru^{III}(boptz^{2-})Ru^{III} species $\mathbf{2}^{4+}$ produces weak absorptions between 900 and 1500 nm and a hypsochromic shift of the charge-transfer band in the visible region. Reduction to the Ru^{II}(boptz$^{\bullet 3-}$)Ru^{II} intermediate $\mathbf{2}^{+}$ causes a hypsochromic shift of the long-wavelength bands as pointed out above for the related tetrazine radical complex $\mathbf{1}^{-}$.

The complex $\mathbf{3}^{2+}$ ion exhibits multiple MLCT bands in the visible region in agreement with the Ru^{II}(boptz^{2-})Ru^{II} formulation and with the presence of π-accepting tetrazine and pap ligands (Figure 7). Oxidation on the timescale of the spectroelectrochemistry experiment (approximately 1 min) shows an only partially reversible spectral change with increasing bands at 488 and 655 nm, indicative of phenoxyl radicals,[7] and in the NIR region at 1105 nm, as has been observed before for transition-metal phenoxyl compounds.[7]

Reduction to a Ru^{II}(boptz$^{\bullet 3-}$)Ru^{II} species $\mathbf{3}^{+}$ decreases the MLCT bands; however, a low-energy broad band appears now at 1600 nm (Figure 7b) that is assigned to an interligand charge-transfer (LLCT) transition from the singly occupied MO (SOMO) at boptz$^{\bullet 3-}$ to the π* molecular orbitals (LUMO) of pap.[25] These features remain after the second reduction, which is likely to occur at one of the pap terminal ligands.

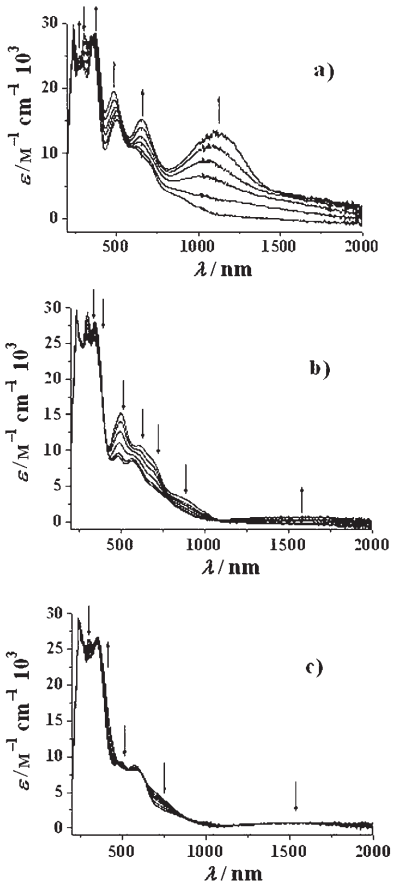

Figure 7. UV-visible-NIR spectroelectrochemistry for the conversions: a) $\mathbf{3}^{2+}\rightarrow\mathbf{3}^{3+}/\mathbf{3}^{4+}$, b) $\mathbf{3}^{2+}\rightarrow\mathbf{3}^{+}$, and c) $\mathbf{3}^{+}\rightarrow\mathbf{3}$ in $CH_3CN/0.1\,M$ Bu_4NPF_6.

Conclusions

The following Scheme 2 summarizes the oxidation state assignments made above for complexes $[L_2Ru(\mu\text{-boptz})RuL_2]^n$.

A comparison between the three systems $\mathbf{1}^n$, $\mathbf{2}^n$, and $\mathbf{3}^n$ is particularly revealing for the question of how external factors, here the terminal ligands, can influence the oxidation state situation in the metal–bridge–metal core. Two extremes are highlighted in the following.

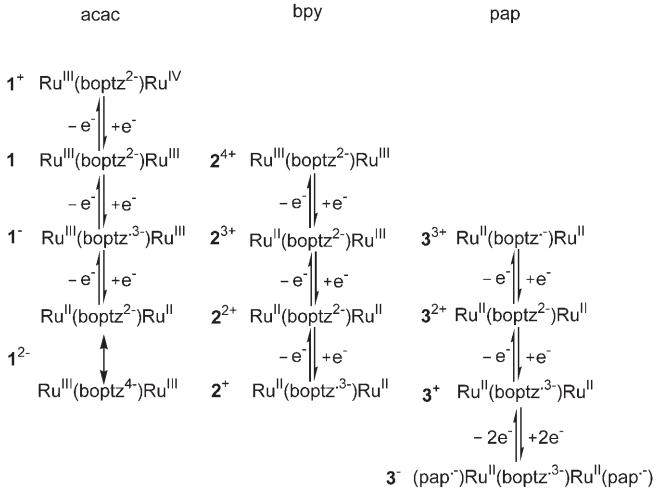

Scheme 2.

1) The $Ru^{II}(boptz^{2-})Ru^{II}$ state is the isolation form for complexes $\mathbf{2}^{2+}$ and $\mathbf{3}^{2+}$, it can also be invoked for complex $\mathbf{1}^{2-}$.
2) In contrast to the stable state $Ru^{II}(boptz^{2-})Ru^{II}$ the intermediate one-electron-oxidized forms differ substantially, the oxidation state being determined by the effect of the ancillary ligands on the metal.

The donating acetylacetonato co-ligands strongly favor the Ru^{III} oxidation state, leading to a species $\mathbf{1}^{-}$ best formulated as $Ru^{III}(boptz^{\bullet 3-})Ru^{III}$.

The strongly π-accepting pap terminal ligands act to maintain a +2 oxidation state on ruthenium, leaving the phenolate-containing bridging ligand to be oxidized from $\mathbf{3}^{2+}$ to a labile phenoxyl species $\mathbf{3}^{3+}$, formulated as $Ru^{II}(boptz^{\bullet -})Ru^{II}$.

Only the moderately π-accepting bpy ancillary ligands allow both Ru^{III} and Ru^{II} states to exist in the then mixed-valent intermediate $\mathbf{2}^{3+}$, formulated as $Ru^{III}(boptz^{2-})Ru^{II}$ or, better, as the valence-averaged $Ru^{2.5}(boptz^{2-})Ru^{2.5}$ species.

Thus, it appears that the ubiquitous use of the bpy co-ligands in ruthenium mixed-valence chemistry[3,17] relies on a lucky choice: 2,2′-bipyridine exhibits an excellent tolerance for both the Ru^{III} and Ru^{II} oxidation states, as demonstrated here by the adoption of the mixed-valent form in $[L_2Ru(\mu\text{-boptz})RuL_2]^{3+}$ with L = bpy. In contrast, the analogous system containing the better π-accepting co-ligand pap stabilizes only the Ru^{II} states to yield a ligand containing a phenoxyl radical, while the corresponding compound with the donor ligand $L = acac^-$ contains two Ru^{III} centers connected by a tetrazine radical-anion bridge. These unprecedented observations have been made possible only through the judicious design and use of a bis(chelated) ligand that contains both (tetrazine) acceptor and (phenolate) donor functions. Such donor–acceptor bifunctional bridges were shown before to have unusual metal–metal mediating properties,[9m] and developments in this direction will thus continue.

Experimental Section

We prepared the starting complexes $[Ru(acac)_2(CH_3CN)_2]$,[26] $[Ru(bpy)_2Cl_2]\cdot 2H_2O$,[27] and $[Ru(pap)_2Cl_2]$[28] according to the reported procedures. 2-Hydroxybenzonitrile was obtained from Aldrich. Other chemicals and solvents were reagent-grade and used as received. For spectroscopic and electrochemical studies HPLC-grade solvents were used.

UV-visible-NIR spectroelectrochemical studies were performed in $CH_3CN/0.1\,M$ Bu_4NPF_6 at 298 K with an OTTLE cell[23] mounted in the sample compartment of a Bruins Instruments Omega 10 spectrophotometer. FTIR spectra were taken on a Nicolet spectrophotometer with samples prepared as KBr pellets. Solution electrical conductivity was checked by using a Systronic 305 conductivity bridge. ^1H NMR spectra were obtained with a 300 MHz Varian FT spectrometer. The EPR measurements were made in a two-electrode capillary tube[29] with an X-band (9.5 GHz) Bruker system ESP300, equipped with a Bruker ER035M gaussmeter

and a HP 5350B microwave counter. Cyclic voltammetric, differential pulse voltammetric, and coulometric measurements were carried out by using a PAR model 273A electrochemistry system. We used platinum-wire working and auxiliary electrodes, and an aqueous saturated calomel reference electrode (SCE) in a three-electrode configuration. The supporting electrolyte was Et_4NClO_4 (0.1 M) and the solute concentration was approximately 10^{-3} M. The half-wave potential E^{o}_{298} was set equal to $0.5(E_{pa}+E_{pc})$, in which E_{pa} and E_{pc} are anodic and cathodic cyclic voltammetric peak potentials, respectively. A platinum-wire gauze working electrode was used in coulometric experiments. The elemental analysis was carried out with a Perkin–Elmer 240C elemental analyser. ESI mass spectra were recorded on a Micromass Q-ToF mass spectrometer.

CAUTION! Perchlorate salts of metal complexes are generally explosive. Care should be taken while handling such complexes.

3,6-Bis(2-hydroxyphenyl)-1,4-dihydro-1,2,4,5-tetrazine (H_4boptz): 2-Hydroxybenzonitrile (1.0 g, 8.39 mmol) and hydrazine hydrate (1.27 g, 1.3 mL, 25.44 mmol, 95%) were dissolved in ethanol (20 mL) and the mixture was heated to reflux for 6 h. The reaction mixture was then cooled at 0 °C overnight and the resulting orange precipitate was filtered off and washed thoroughly with cold ethanol. The product was recrystallized from hot ethanol. Yield: 0.80 g (71%); m.p. 258 °C; ESI MS (in CH_2Cl_2): m/z calcd for $[(H_4boptz)]^+$: 268.09; found 269.15; elemental analysis calcd (%) for $C_{14}H_{12}N_4O_2$: C 62.68, H 4.51, N 20.88; found: C 62.32, H 4.61, N 19.18; ^{1}H NMR (300 MHz, $CDCl_3$, 298 K): $\delta = 11.34$ (s, 1H; OH), 9.40 (s, 1H; NH), 7.72 (d, $J = 4.8$ Hz, 1H), 7.36 (t, $J = 6.0$ Hz, 1H), 6.95 ppm (m, 2H).

3,6-Bis(2-hydroxyphenyl)-1,2,4,5-tetrazine (H_2boptz): Nitric oxide (NO) gas was purged into a solution of H_4boptz (0.10 g, 0.37 mmol) in CH_2Cl_2 (15 mL) for 1 h. The red solution formed was evaporated to dryness. The product was then purified by using a silica gel column (60–120 mesh) with CH_2Cl_2/CH_3CN (10:1 v/v) as eluent. Yield: 0.094 g (95%); m.p. 222 °C; ESI MS (in CH_3OH): m/z calcd for $[(H_2boptz)]^+$: 266.08; found: 267.14; elemental analysis calcd (%) for $C_{14}H_{10}N_4O_2$: C 63.15, H 3.79, N 21.04; found: C 63.66, H 3.09, N 19.57; ^{1}H NMR (300 MHz, $(CD_3)_2SO$, 298 K): $\delta = 10.73$ (s, 1H; OH), 8.27 (t, $J = 4.5$ Hz, 1H), 7.56 (t, $J = 5.7$ Hz, 1H), 7.13 ppm (m, 2H).

$[(acac)_2Ru(\mu\text{-boptz})Ru(acac)_2]$ (1): $[Ru(acac)_2(CH_3CN)_2]$ (0.10 g, 0.26 mmol), H_2boptz (0.035 g, 0.13 mmol), and sodium acetate (0.03 g, 0.36 mmol) were heated to reflux in ethanol (20 mL) for 8 h. The initially transparent orange solution gradually changed to dark brown. The solid mass obtained on removal of the solvent under reduced pressure was dissolved in the minimum volume of CH_2Cl_2 and purified by using a silica gel (60–120 mesh) column with CH_2Cl_2/CH_3CN (20:1 v/v) as eluent. Yield: 0.057 g (50%); ESI MS (in CH_2Cl_2): m/z calcd for $[\mathbf{1}]^+$: 864.05; found: 864.07 (see also Figure S2a in the Supporting Information); elemental analysis calcd (%) for $C_{34}H_{36}N_4O_{10}Ru_2$: C 47.33, H 4.21, N 6.49; found: C 47.69, H 4.21, N 6.28.

$[(bpy)_2Ru(\mu\text{-boptz})Ru(bpy)_2](ClO_4)_2$ (2-$(ClO_4)_2$): A mixture of $[Ru(bpy)_2Cl_2]\cdot 2H_2O$ (0.10 g, 0.19 mmol) and $AgClO_4$ (0.10 g, 0.48 mmol) in ethanol (10 mL) was heated to reflux with constant stirring for 2 h under a dinitrogen atmosphere. The resultant AgCl precipitate was filtered off after cooling, leaving a red solution of $[Ru(bpy)_2(EtOH)_2]^{2+}$. We added H_2boptz (0.025 g, 0.09 mmol) and sodium acetate (0.025 g, 0.30 mmol), and the mixture was refluxed for 6 h under dinitrogen atmosphere. During the course of the reaction the initial red color changed to purple. The solution was then evaporated to dryness under reduced pressure and the obtained solid mass was purified on an alumina chromatography column (neutral) for purification. The purple solution containing **2**-$(ClO_4)_2$ was eluted with CH_2Cl_2/CH_3CN (2:1 v/v). Yield: 0.057 g (45%); ESI MS (in CH_3CN): m/z calcd for $[\mathbf{2}\text{-}(ClO_4)]^+$: 1191.09; found: 1191.11 (see also Figure S2b in the Supporting Information); elemental analysis calcd (%) for $C_{54}H_{40}Cl_2N_{12}O_{10}Ru_2$: C 50.23, H 3.12, N 13.03; found: C 49.89, H 3.18, N 12.71.

$[(pap)_2Ru(\mu\text{-boptz})Ru(pap)_2](ClO_4)_2$ (3-$(ClO_4)_2$): $[Ru(pap)_2Cl_2]$ (0.10 g, 0.198 mmol) and $AgClO_4$ (0.10 g, 0.48 mmol) were heated to reflux in ethanol (10 mL) for 2 h under a dinitrogen atmosphere. The precipitated AgCl was filtered off leaving a purple solution of $[Ru(pap)_2(EtOH)_2]^{2+}$. We added H_2boptz (0.025 g, 0.09 mmol) and sodium acetate (0.025 g, 0.30 mmol) to this purple solution and the mixture was refluxed for 4 h under dinitrogen. The resultant purple solution was evaporated to dryness under reduced pressure and the solid mass was purified by chromatography with a silica gel column (60–120 mesh) with CH_2Cl_2/CH_3CN (5:1 v/v). Yield: 0.083 g (60%); ESI MS (in CH_3CN): m/z calcd for $[\mathbf{3}\text{-}(ClO_4)]^+$: 1298.68; found: 1299.20 (see also Figure S2c in the Supporting Information); elemental analysis calcd (%) for $C_{58}H_{44}Cl_2N_{16}O_{10}Ru_2$: C 49.83, H 3.17, N 16.03; found: C 49.49, H 3.05, N 15.53.

Magnetic susceptibility measurements: The variable-temperature magnetic susceptibility data were measured on a Quantum Design MPMSXL SQUID susceptometer over a temperature range of 2–300 K. Each raw data field was corrected for the diamagnetic contribution of both the sample holder and the complex to the susceptibility. The molar diamagnetic corrections were calculated on the basis of Pascal constants. The fitting of the experimental data was carried out by using the commercial MATLAB V.5.1.0.421 program.

X-ray crystal structure analysis: Single-crystals of H_2boptz were grown by slow diffusion of a solution of the compound in dichloromethane into hexane, followed by slow evaporation. X-ray diffraction data of H_2boptz were collected on a PC-controlled Enraf-Nonius CAD-4 (MACH-3) single-crystal X-ray diffractometer by using $Mo_{K\alpha}$ radiation. The structure was solved and refined by full-matrix least-squares on F^2 by using SHELX-97 (SHELXTL).[30] Hydrogen atoms were included in the refinement process as per the riding model.

CCDC 266312 contains the supplementary crystallographic data for H_2boptz in this paper. These data can be obtained free of charge from the Cambridge Crystallographic Data Centre via www.ccdc.cam.ac.uk/data_request/cif.

Acknowledgements

We are grateful to the DST, New Delhi (India) and the DAAD and the DFG (Germany) for financial support. The X-ray structural study was carried out at the National Single-Crystal Diffractometer Facility, Indian Institute of Technology Bombay (India).

[1] a) H. Taube, *Angew. Chem.* **1984**, *96*, 315; *Angew. Chem. Int. Ed. Engl.* **1984**, *23*, 329; b) J. K. Kochi, *Organometallic Mechanisms and Catalysis*, Academic Press, New York, **1978**.

[2] D. Astruc, *Electron Transfer and Radical Processes in Transition-Metal Chemistry*, Wiley-VCH, New York, **1995**.

[3] K. D. Demadis, C. M. Hartshorn, T. J. Meyer, *Chem. Rev.* **2001**, *101*, 2655.

[4] W. Kaim, A. Klein, M. Glöckle, *Acc. Chem. Res.* **2000**, *33*, 755.

[5] R. J. Crutchley, *Adv. Inorg. Chem.* **1999**, *41*, 273.

[6] a) S. Kar, B. Pradhan, R. K. Sinha, T. Kundu, P. Kodgire, K. K Rao, V. G. Puranik, G. K. Lahiri, *Dalton Trans.* **2004**, 1752; b) N. Chanda, R. H. Laye, S. Chakraborty, R. L. Paul, J. C. Jeffery, M. D. Ward, G. K. Lahiri, *J. Chem. Soc. Dalton Trans.* **2002**, 3496; c) B. Mondal, H. Paul, V. G. Puranik, G. K. Lahiri, *J. Chem. Soc. Dalton Trans.* **2001**, 481; d) B. Mondal, M. G. Walawalkar, G. K. Lahiri, *J. Chem. Soc. Dalton Trans.* **2000**, 4209; e) A. Bharath, B. K. Santra, P. Munshi, G. K. Lahiri, *J. Chem. Soc. Dalton Trans.* **1998**, 2643; f) B. K. Santra, G. K. Lahiri, *J. Chem. Soc. Dalton Trans.* **1998**, 1613; g) B. K. Santra, G. K. Lahiri, *J. Chem. Soc. Dalton Trans.* **1998**, 139; h) B. K. Santra, G. K. Lahiri, *J. Chem. Soc. Dalton Trans.* **1997**, 1883; i) B. K. Santra, M. Menon, C. K. Pal, G. K. Lahiri, *J. Chem. Soc. Dalton Trans.* **1997**, 1387; j) B. K. Santra, G. K. Lahiri, *J. Chem. Soc. Dalton Trans.* **1997**, 129; k) B. K. Santra, G. A. Thakur, P. Ghosh, A. Pramanik, G. K. Lahiri, *Inorg. Chem.* **1996**, *35*, 3050.

[7] a) E. Bill, E. Bothe, P. Chaudhuri, K. K. Chlopek, D. Herebian, S. Kokatam, K. Roy, T. Weyhermüller, F. Neese, K. Wieghardt, *Chem. Eur. J.* **2005**, *11*, 204; b) P. Chaudhuri, K. Wieghardt, *Prog. Inorg. Chem.* **2001**, *50*, 151; c) S. Kimura, E. Bill, E. Bothe, T. Weyhermüller, K. Wieghardt, *J. Am. Chem. Soc.* **2001**, *123*, 6025; d) J. Müller,

A. Kikuchi, E. Bill, T. Weyhermüller, P. Hildebrandt, L. Ould-Moussa, K. Wieghardt, *Inorg. Chim. Acta* **2000**, *297*, 265; e) E. Bill, J. Müller, T. Weyhermüller, K. Wieghardt, *Inorg. Chem.* **1999**, *38*, 5795; f) P. Chaudhuri, M. Hess, J. Müller, K. Hildenbrand, E. Bill, T. Weyhermüller, K. Wieghardt, *J. Am. Chem. Soc.* **1999**, *121*, 9599; g) M. D. Snodin, L. Ould-Moussa, U. Wallmann, S. Lecomte, V. Bachler, E. Bill, H. Hummel, T. Weyhermüller, P. Hildebrandt, K. Wieghardt, *Chem. Eur. J.* **1999**, *5*, 2554; h) R. Schnepf, A. Sokolowski, J. Müller, V. Bachler, K. Wieghardt, P. Hildebrandt, *J. Am. Chem. Soc.* **1998**, *120*, 2352; i) "Spectroscopy of Biological Molecules: Modern Trends": R. Schnepf, P. Hildebrandt, A. Sokolowski, J. Müller, K. Weighardt, 7th European Conference on Spectroscopy of Biological Molecules, Madrid (Spain) **1997**, Abstract 189; j) A. Sokolowski, J. Müller, T. Weyhermüller, R. Schnepf, P. Hildebrandt, K. Hildenbrand, E. Bothe, K. Wieghardt, *J. Am. Chem. Soc.* **1997**, *119*, 8889; k) B. Adam, E. Bill, E. Bothe, B. Goerdt, G. Haselhorst, K. Hildenbrand, A. Sokolowski, S. Steenken, T. Weyhermüller, K. Wieghardt, *Chem. Eur. J.* **1997**, *3*, 308; l) A. Sokolowski, E. Bothe, E. Bill, T. Weyhermüller, K. Wieghardt, *Chem. Commun.* **1996**, 1671; m) J. Hockertz, S. Steenken, K. Wieghardt, P. Hildebrandt, *J. Am. Chem. Soc.* **1993**, *115*, 11222.

[8] W. Kaim, *Coord. Chem. Rev.* **2002**, *230*, 127.

[9] a) J. E. Johnson, C. De Graff, R. R. Ruminski, *Inorg. Chim. Acta* **1991**, *187*, 73; b) J. Poppe, M. Moscherosch, W. Kaim, *Inorg. Chem.* **1993**, *32*, 2640; c) V. Kasack, W. Kaim, H. Binder, J. Jordanov, E. Roth, *Inorg. Chem.* **1995**, *34*, 1924; d) S. Chellamma, M. Liebermann, *Inorg. Chem.* **2001**, *40*, 3177; e) S. Roche, J. A. Thomas, L. J. Yellowlees, *Chem. Commun.* **1998**, 1429; f) P. A. Stuzhin, S. I. Vagin, M. Hanack, *Inorg. Chem.* **1998**, *37*, 2655; g) S. Kohlmann, S. Ernst, W. Kaim, *Angew. Chem.* **1985**, *97*, 698; *Angew. Chem. Int. Ed. Engl.* **1985**, *24*, 684; h) S. Ernst, V. Kasack, W. Kaim, *Inorg. Chem.* **1988**, *27*, 1146; i) S. D. Ernst, W. Kaim, *Inorg. Chem.* **1989**, *28*, 1520; j) Q. Jaradat, K. Barqawi, T. S. Akaseh, *Inorg. Chim. Acta* **1986**, *116*, 63; k) M. H. Zaghal, H. A. Qaseer, *Inorg. Chim. Acta* **1989**, *163*, 193; l) K. C. Gordon, A. K. Burrel, T. J. Simpson, S. E. Page, G. Kelso, M. I. J. Polson, A. Flood, *Eur. J. Inorg. Chem.* **2002**, 554; m) B. Sarkar, W. Kaim, A. Klein, B. Schwederski, J. Fiedler, C. Duboc-Toia, G. K. Lahiri, *Inorg. Chem.* **2003**, *42*, 6172; n) B. Sarkar, R. H. Laye, B. Mondal, S. Chakraborty, R. L. Paul, J. C. Jeffery, V. G. Puranik, M. D. Ward, G. K. Lahiri, *J. Chem. Soc. Dalton Trans.* **2002**, 2097; o) W. Kaim, J. Fees, *Z. Naturforsch. B* **1995**, *50*, 123; p) M. Glöckle, J. Fiedler, W. Kaim, *Z. Anorg. Allg. Chem.* **2001**, *627*, 1441; q) M. Glöckle, K. Hübler, H.-J. Kümmerer, G. Denninger, W. Kaim, *Inorg. Chem.* **2001**, *40*, 2263; r) B. Sarkar, S. Frantz, W. Kaim, C. Duboc, *Dalton Trans.* **2004**, 3727; s) S. Patra, B. Sarkar, S. Ghumaan, J. Fiedler, W. Kaim, G. K. Lahiri, *Inorg. Chem.* **2004**, *43*, 6108; t) A. Singh, N. Singh, D. S. Pandey, *J. Organomet. Chem.* **2002**, *642*, 48.

[10] a) S. Ernst, V. Kasack, W. Kaim, *Inorg. Chem.* **1988**, *27*, 1146; b) L. S. Kelso, D. A. Reitsma, F. R. Keene, *Inorg. Chem.* **1996**, *35*, 5144.

[11] C. J. O'Connor, *Prog. Inorg. Chem.* **1982**, *29*, 203.

[12] R. Schneider, T. Weyhermüller, K. Wieghardt, B. Nuber, *Inorg. Chem.* **1993**, *32*, 4925.

[13] S. Kar, N. Chanda, S. M. Mobin, A. Datta, F. A. Urbanos, V. G. Puranik, R. Jimenez-Aparicio, G. K. Lahiri, *Inorg. Chem.* **2004**, *43*, 4911.

[14] a) Y. Mikata, N. Takeshita, T. Miyazu, Y. Miyata, T. Tanase, I. Kinoshita, A. Ichimura, W. Mori, S. Takamizawa, S. Yano, *J. Chem. Soc. Dalton Trans.* **1998**, 1969; b) M. Obata, N. Tanihara, M. Nakai, M. Harada, S. Aimoto, I. Yamazaki, A. Ichimura, I. Kinoshita, M. Mikuriya, M. Hoshino, S. Yano, *Dalton Trans.* **2004**, 3283.

[15] a) N. Chanda, B. Sarkar, S. Kar, J. Fiedler, W. Kaim, G. K. Lahiri, *Inorg. Chem.* **2004**, *43*, 5128; b) S. Ghumaan, B. Sarkar, S. Patra, K. Parimal, J. van Slageren, J. Fiedler, W. Kaim, G. K. Lahiri, *Dalton Trans.* **2005**, 706; c) S. Patra, B. Sarkar, S. M. Mobin, W. Kaim, G. K. Lahiri, *Inorg. Chem.* **2003**, *42*, 6469; d) A. Nayak, S. Patra, B. Sarkar, S. Ghumaan, V. G. Puranik, W. Kaim, G. K. Lahiri, *Polyhedron* **2005**, *24*, 333; e) N. Chanda, B. Sarkar, J. Fiedler, W. Kaim, G. K. Lahiri, *Dalton Trans.* **2003**, 3550.

[16] Y. Hoshino, S. Higuchi, J. Fiedler, C.-Y. Su, A. Knödler, B. Schwederski, B. Sarkar, H. Hartmann, W. Kaim, *Angew. Chem.* **2003**, *115*, 698; *Angew. Chem. Int. Ed.* **2003**, *42*, 674.

[17] C. Creutz, *Prog. Inorg. Chem.* **1983**, *30*, 1.

[18] a) M. B. Robin, P. Day, *Adv. Inorg. Chem. Radiochem.* **1967**, *10*, 247; b) M. D. Ward, *Chem. Soc. Rev.* **1995**, *24*, 121; c) J. A. McCleverty, M. D. Ward, *Acc. Chem. Res.* **1998**, *31*, 842; d) T. Scheiring, J. A. Olabe, A. R. Parise, J. Fiedler, W. Kaim, *Inorg. Chim. Acta* **2000**, *300–302*, 125.

[19] For a detailed discussion of three-spin systems see: a) S. Ye, B. Sarkar, F. Lissner, T. Schleid, J. van Slageren, J. Fiedler, W. Kaim, *Angew. Chem.* **2005**, *117*, 2140; *Angew. Chem. Int. Ed.* **2005**, *44*, 2103; b) S. Ghumaan, B. Sarkar, S. Patra, J. Fiedler, J. van Slageren, W. Kaim, G. K. Lahiri, *Inorg. Chem.* **2005**, *44*, 3210.

[20] W. Kaim, S. Ernst, S. Kohlmann and P. Welkerling, *Chem. Phys. Lett.* **1985**, *118*, 431.

[21] a) S. Chakraborty, R. H. Laye, R. L. Paul, R. G. Gonnade, V. G. Puranik, M. D. Ward, G. K. Lahiri, *J. Chem. Soc. Dalton Trans.* **2002**, 1172; b) S. Chakraborty, R. H. Laye, P. Munshi, R. L. Paul, M. D. Ward, G. K. Lahiri, *J. Chem. Soc. Dalton Trans.* **2002**, 2348; c) S. Kar, T. A. Miller, S. Chakraborty, B. Sarkar, B. Pradhan, R. K. Sinha, T. Kundu, M. D. Ward, G. K. Lahiri, *Dalton Trans.* **2003**, 2591.

[22] a) M. Kaupp, T. Gress, R. Reviakine, O. L. Malkina, V. G. Malkin, *J. Phys. Chem. B* **2003**, *107*, 331; b) S. Un, C. Gerez, E. Elleingand, M. Fontecave, *J. Am. Chem. Soc.* **2001**, *123*, 3048.

[23] M. Krejcik, M. Danek, F. Hartl, *J. Electroanal. Chem. Interfacial Electrochem.* **1991**, *317*, 179.

[24] a) A.-C. Ribou, J.-P. Launay, K. Takahashi, T. Nihira, S. Tarutani, C. W. Spangler, *Inorg. Chem.* **1994**, *33*, 1325; b) C. Patoux, J.-P. Launay, M. Belay, S. Chaodorowski-Kimmes, J.-P. Colin, J. Stuart, J.-P. Sauvage, *J. Am. Chem. Soc.* **1998**, *120*, 3177.

[25] a) N. C. Fletcher, T. C. Robinson, A. Behrendt, J. C. Jeffery, Z. R. Reeves, M. D. Ward, *J. Chem. Soc. Dalton Trans.* **1999**, 2999; b) A. K. Ghosh, S.-M. Peng, R. L. Paul, M. D. Ward, S. Goswami, *J. Chem. Soc. Dalton Trans.* **2001**, 336; c) P. R. Auburn, A. B. P. Lever, *Inorg. Chem.* **1990**, *29*, 2551; d) G. A. Heath, L. J. Yellowlees, P. S. Braterman, *Chem. Phys. Lett.* **1982**, *92*, 646.

[26] T. Kobayashi, Y. Nishina, K. G. Shimizu, G. P. Satô, *Chem. Lett.* **1988**, 1137.

[27] B. P. Sullivan, D. J. Salmon, T. J. Meyer, *Inorg. Chem.* **1978**, *17*, 3334.

[28] S. Goswami, A. R. Chakravorty, A. Chakravorty, *Inorg. Chem.* **1981**, *20*, 2246.

[29] W. Kaim, S. Ernst, V. Kasack, *J. Am. Chem. Soc.* **1990**, *112*, 173.

[30] G. M. Sheldrick, SHELX-97, Program for Crystal Structure Solution and Refinement, University of Göttingen, Göttingen (Germany), **1997**.

Received: March 16, 2005
Published online: August 31, 2005

